Polymer 49 (2008) 4332–4343

Contents lists available at ScienceDirect

Polymer

journal homepage: www.elsevier.com/locate/polymer

UV-photopolymerisation of poly(methyl methacrylate)-based inorganic–organic hybrid coatings and bulk samples reinforced with methacrylate-modified zirconium oxocluster

Francesco Graziola [a,b], Fabrizio Girardi [b], Matthias Bauer [c], Rosa Di Maggio [b], Mauro Rovezzi [d], Helmut Bertagnolli [c], Cinzia Sada [e], Gilberto Rossetto [f], Silvia Gross [a,*]

[a] ISTM-CNR, Dipartimento di Scienze Chimiche, Università degli Studi di Padova, and INSTM, via Marzolo, 1, Padova, 35131, Italy
[b] Dipartimento di Ingegneria dei Materiali e Tecnologie Industriali, Università di Trento, via Mesiano, 77, Trento, 38100, Italy
[c] Institut für Physikalische Chemie, Universität Stuttgart, Pfaffenwaldring 55, D-70569 Stuttgart, Germany
[d] CNR-INFM-OGG GILDA CRG c/o ESRF, 6 Rue Jules Horowitz F-38043 Grenoble, France
[e] Dipartimento di Fisica "Galileo Galilei", Università degli Studi di Padova, via Marzolo 9, Padova, 35131, Italy
[f] ICIS-CNR, Corso Stati Uniti, 4 – 35127 Padova, Italy

ARTICLE INFO

Article history:
Received 14 March 2008
Received in revised form 1 August 2008
Accepted 4 August 2008
Available online 9 August 2008

Keywords:
Polymer materials
Polymer science and technology
Polymer composite materials

ABSTRACT

In this work, we developed and optimised a synthetic route which enables to produce by spray-coating hard, transparent and stable inorganic–organic hybrid coatings for a wide variety of different substrates (e.g. stone, stainless steel, polymethylmethacrylate, polyethylene, wood, anodized aluminum). Chemically and thermally stable acrylate-based hybrid materials embedding the zirconium oxocluster $Zr_4O_2(OMc)_{12}$, OMc=(CH_2=$C(CH_3)C(O)O$) were prepared and UV-cured.
The coatings of different compositions on different substrates were characterized by numerous analytical and spectroscopic methods such as FT-IR spectroscopy, Angle Resolved-XPS (AR-XPS), Secondary Ion Mass Spectrometry (SIMS), X-ray Absorption Spectroscopy (XAS), Environmental Scanning Electron Microscopy (ESEM) and Energy Dispersive X-ray analysis (EDX). Bulk samples were also prepared for additional characterizations. The bulk samples were analysed by FT-IR, whereas the cross-linking degree was qualitatively evaluated by swelling experiments. As far as the mechanical properties are concerned, the shear storage modulus (G') and loss modulus (G'') were measured by Dynamical Mechanical Thermal Analysis (DMTA) technique. Moreover, the best conditions for the curing and cross-linking processes of the hybrid materials were studied up to 200 °C by using Differential Scanning Calorimetry (DSC). The thermal stability of the hybrid samples was evaluated by Thermogravimetric Analysis (TGA).

1. Introduction

Inorganic–organic hybrid materials in the form of thin or thick layers have attracted considerable attention in recent years due to improvements achieved in various coating properties, including resistance to scratch, abrasion, heat stability, as well as other mechanical properties [1–9].

The properties of hybrid materials are determined by the chemical nature of the individual organic and inorganic components, as well as by their interaction at the interphase. In particular, molecular level intermixing can be achieved through the formation of strong covalent chemical bonds among the inorganic and organic building blocks [2,3,7].

To this aim, the use of organically functionalised oxoclusters, which can be grafted to the forming polymer matrix through formation of covalent bonds, has been proven to be a suitable approach to achieve a better control of the dispersion of the inorganic building blocks into the organic backbone [7,8]. Several acrylate- and methacrylate-substituted oxometallate clusters (based on Ti, Zr, Hf, Ta, Nb, Y, Mn, mixed Ba–Ti, Ti–Hf, Zr–Ti) were prepared by Schubert et al. [6,7,10–24] by reacting the alkoxide with an excess of methacrylic or acrylic acid. More recently, the preparation of oxoclusters functionalised with other groups such as norbornene [25] or thiols [26] has also been successfully addressed. Inorganic–organic hybrid materials have been prepared by cross-linking suitable organic monomers (such as styrene, methylmethacrylate, ethylacrylate, polyethyleneglycol diacrylate etc.) with these inorganic functionalised oxoclusters through free radical polymerisation process [2,3,6,7,11,14,18,20,21,25–41].

* Corresponding author. Tel.: +39 049 8275736; fax: +39 049 8275161.
E-mail address: silvia.gross@unipd.it (S. Gross).

0032-3861/$ – see front matter © 2008 Elsevier Ltd. All rights reserved.
doi:10.1016/j.polymer.2008.08.005

Furthermore, inorganic–organic hybrids based on nanoparticles of zirconia covalently linked to the organic polymer network have also been prepared by the radical polymerisation of 2-hydroxyethyl methacrylate (HEMA) modified by $Zr(OR)_4$ and acetylacetone. In this case, the polymerisation was initiated by dibenzoyl peroxide and occurred at room temperature without any heating, so that zirconium ions have been proposed to catalyze the formation of radicals [42]. Instead, in the absence of dibenzoyl peroxide as initiator, the polymerisation occurs by a different ionic mechanism [43].

The preparation of these hybrid materials has been mainly addressed by using thermo-activated free radical polymerisation [7,10,14,19–21,25,28–30,32,34–40,42].

Recently, Schubert et al. [25,38,39,68] reported on the investigation of the thermal and mechanical properties of inorganic–organic hybrid materials produced by thermal-activated copolymerisation of zirconium oxocluster with styrene.

In this work, the UV-activated photopolymerisation was instead adopted to photopolymerise the methacrylate-functionalised zirconium oxocluster $Zr_4O_2(OMc)_{12}$, $OMc{=}(CH_2{=}C(CH_3)C(O)O)$ with methylmethacrylate. Experimental parameters such as the amount of the clusters and the polymerisation conditions were selectively changed to investigate their effect on the properties of the hybrid materials. The general properties of the UV-cured nanostructured hybrid acrylic coatings based on the methacrylate-modified zirconium oxocluster were therefore checked by analysing their morphology, composition and short-range structure as well as their thermal and mechanical properties.

The UV curing method was chosen since it induces the polymer formation with a fast transformation of the liquid monomer into a solid film with tailored physico-chemical and mechanical properties. Since UV curing, in many cases, is a solvent free process, it is usually carried out at room temperature and, due to its higher efficiency and shorter processing times, it has a lower energy consumption with respect to themal-driven processes, it can be considered more environmental friendly than other curing methods [44]. These are some of the main reasons why it began to be widely exploited in the coatings technology [45].

In the past, we have already used photopolymerisation to prepare inorganic–organic hybrid layers to be used as dielectric layers and we investigated their dielectric properties [29,32,35,46]. Recently we have also studied the thermomechanical properties of coatings produced by copolymerisation of the zirconium oxocluster $Zr_4O_2(OMc)_{12}$ with the resin polyethyleneglycol diacrylate [41].

In the present work we present a further progress in this field. In particular, a polymerisation procedure was set and optimised; it is based on the spray-coating deposition and simultaneous photopolymerisation of a suitable formulation of monomer, cluster and initiator on a substrate.

This method, based on simultaneous deposition and curing, allows obtaining transparent and homogeneous layers. Moreover, the large number of analytical methods applied to investigate the synthesized samples permitted to elucidate the physical, chemical and structural properties of the coatings and to assert the optimised process parameters.

To investigate the mechanical properties of the materials, bulk samples were also prepared by using the same experimental parameters applied to prepare the coatings.

2. Experimental

2.1. Materials

The zirconium oxocluster $Zr_4O_2(OMc)_{12}$ (Zr4) bearing twelve methacrylic functionalities was synthesized according to the previously reported procedure [14] starting from zirconium butoxide and methacrylic acid in butoxide:acid 1:7 molar ratio, as reported in the quoted reference. Zirconium butoxide ($Zr(OBu)_4$) 80 wt% in butanol, was purchased from Aldrich. Methacrylic acid 99%, purchased from Aldrich, was distilled under reduced pressure. All the chemicals were stored under argon, while the solvents were additionally stored on molecular sieves. All operations for the synthesis of the cluster were performed under argon using standard Schlenk techniques.

IRGACURE 819 (phenyl-bis-(2,4,6-trimethylbenzoyl)phosphine oxide), kindly gifted by Ciba Speciality Chemicals Inc. (Basel, Switzerland) was employed as photoinitiator at 4.2 wt% concentration with respect to the monomer.

2.2. Sample preparation

The used substrates were wood, anodized aluminium, stone, stainless steel, polymethylmethacrylate, polyethylene. The hybrid coatings were also deposited on silicon wafer (Si (100) p-type, boron-doped) to investigate them by IR spectroscopy.

Before deposition, the substrates were cleaned and rinsed both in detergent, doubly distilled water, and 2-propanol. This procedure was repeated several times to remove organic residuals at the surface thus favouring the best adhesion between coating and substrate. The substrates were finally dried in air at room temperature. For wood and stones, the treatment with solvent was replaced by a thermal treatment at 120 °C for 1 h.

To prepare the deposition formulation, the zirconium oxocluster Zr4 was dispersed in the liquid methylmethacrylate monomer in a Zr4:MMA monomer molar ratio of 1:50, 1:100, 1:200.

Irgacure 819 photoinitiator (4.2 wt% with respect to the monomer) was added to the obtained mixtures. Selected experiments were also carried out with a half and a two-fold amounts of initiator (i.e. 2.1 and 8.4 wt%, respectively).

The liquid formulation was spray-coated onto the different substrates using an air-brush Paasch Model VLS. The operating pressure was 700 mbar. The films were photopolymerised during deposition under a UV lamp (Helios Italquarz s.r.l. 125 W, 230 V and an emission range of 250–450 nm) for 10 min, a time optimised on the basis of the time-resolved IR measurements (*vide infra*). The distance between the lamp and the substrate was set to 19 cm.

Bulk samples for thermal and mechanical characterization were also prepared by polymerisation in a cylindrical PE flask (30 × 8 mm), whereas self-supporting films were yielded in a Petri glass. The samples were photopolymerised for 1 h. Selected samples were photopolymerised for 2 h. The UV absorption of the cylindrical PE flask was determined by UV–vis spectra (data not shown) evidencing no remarkable absorption of the flask in the spectral range of emission of the lamp.

2.3. Sample characterization

The surface composition of the films was investigated by XPS. XPS spectra were run on a Perkin-Elmer Φ 5600ci spectrometer using standard Al-K_α radiation (1486.6 eV) operating at 350 W. The working pressure was $<5 \times 10^{-8}$ Pa. The spectrometer was calibrated by assuming the binding energy (BE) of the $Au4f_{7/2}$ line at 83.9 eV with respect to the Fermi level. The standard deviation for the BE values was 0.15 eV. The reported BE were corrected for the charging effects, assigning to the C1s line of carbon the BE value of 284.6 eV [47]. Survey scans (187.85 pass energy, 1 eV/step, 25 ms per step) were obtained in the 0–1350 eV range. Detailed scans (58.7 eV pass energy, 0.1 eV/step, 100 ms per step) were recorded for the O1s, C1s, Zr3p, Zr3d regions. The atomic composition was evaluated after a Shirley type background subtraction [48], using sensitivity factors supplied by Perkin–Elmer [49]. Charge effects were partially compensated by using a charge neutralizer (flood

gun). The assignments of the peaks were carried out by using the values reported in Refs. [47,49–52].

In order to analyse the in-depth composition of selected film samples and to check the in-depth distribution of the zirconium oxocluster in the polymer matrix, AR-XPS measurements (carried out at different take-off angles, i.e. 30°, 45° and 60° with respect to the analyser) and SIMS analyses were performed.

SIMS measurements were carried out on selected film samples by means of an IMS 4f mass spectrometer (Cameca, Padova, Italy) using a 10 kV Cs^+ primary beam and by negative secondary ion detection (the sample potential was fixed at −4.5 kV) with a final impact energy of 14.5 keV. The SIMS spectra were carried out in Ultra High Vacuum conditions at a primary beam intensity equal to 70 nA and rastering over a nominally $125 \times 125\ \mu m^2$ area. Beam blanking mode was used to improve the depth resolution, interrupting the sputtering process during magnet stabilization periods. The charge build-up occurring in insulating samples during the in-depth profiling was compensated by an electron gun without any need to cover the surface with a metal film. The erosion speed was evaluated by measuring the depth of the erosion crater at the end of each analysis by means of a Tencor Alpha Step profilometer with a maximum uncertainty of few nanometers. The dependence of the erosion speed on the matrix composition was taken into account for each sample by recording various spectra at different depths in each sample.

As far as the polymerisation kinetics of the coatings are concerned, FT-IR spectroscopy was exploited: the IR spectra were acquired with a Nexus 870 FTIR spectrometer (Nicolet) in the range from 400 to 4000 cm^{-1}, with a resolution of 4 cm^{-1}, by averaging 64 scans.

XAS measurements were performed on the coating samples at the GILDA beam line (BM08) of the European Synchrotron Radiation Facility (ESRF) in Grenoble, France. XAS measurements were performed at the Zirconium *K*-edge (17.998 keV); the absorption spectra were collected in the fluorescence mode using a dynamically sagitally focusing Si(311) monochromator and a 13-elements hyperpure Ge detector. Digital electronics were used to read out the fluorescence detector. To avoid mistakes in the XANES region due to small changes in the energy calibration between two measurements, all spectra were corrected to the edge position of a zirconium foil, which was measured parallel to the samples between the second and third ionisation chambers. Several spectra were averaged to achieve a better signal to noise ratio. The data analysis was carried out using the procedure reported [53–56], in particular by choosing the Hanning window function of $\Delta R = 2.6$ Å (1.2–3.8 Å) and carrying out the data analysis in *k*-space ($\Delta k = 12$ $Å^{-1}$) on Fourier filtered data to remove noise and multiple scattering contributions. The filtered range was chosen according to the range of significant data and it is given in Table 2 together with the results of the fitting procedure. According to the used data range, the number of independent points is $N_{ind} = (2\Delta k \Delta R/\pi) = 19$ in all spectra. The maximum number of adjusted parameters was 13; therefore a high degree of overdetermacy could be achieved. It gives the ratio of the number of independent points to the number of actually fitted parameters. Adjustment of the common theoretical EXAFS expression was carried out according to the curved wave formalism of the EXCURV98 program with XALPHA phase and amplitude functions [56]. The mean free path of the scattered electrons was calculated from the imaginary part of the potential (VPI set to −4.00 eV). Since XALPHA phases and amplitudes were used, an amplitude reduction factor S_0^2 was necessary to account for inelastic processes [57]. It was determined experimentally for monoclinic ZrO_2 to be 0.8 ± 0.1 by setting the coordination numbers to the crystallographic values. Therefore $S_0^2 = 0.8$ was used for all samples although this assumption introduces the rather large uncertainties in the coordination numbers and Debye–Waller like factors σ. An inner potential correction E_f was introduced when fitting experimental data with theoretical models that accounts for an overall phase shift between the experimental and calculated spectra. Finally the quality of fit is given in terms of the well known *R*-factor according to the literature Ref. [58].

In order to investigate the thermal stability of the bulk hybrid samples, thermal analyses were performed using a Labsys Setaram instrument. For TGA-HT/DSC, a DSC platinum probe was attached to the balance to perform simultaneous TGA (thermogravimetry) and DSC (Differential Scanning Calorimeter) analysis of the same sample. TG and HT-DSC were recorded in the range 20–1000 °C both in air and helium flow (100 ml min^{-1}) with a heating rate of 10 °C min^{-1}.

Moreover, Dynamical Mechanical Thermal Analysis (DMTA) was performed on the bulk samples in shear mode on cured prism having planar and parallel faces with an area of 12 mm^2 and 3.5 mm thick. Two subsequent scans were run up to 200 °C, with a heating rate of 10 °C min^{-1}. Shear storage (G') and loss (G'') modulus were measured by using a Seiko DMS 6100 instrument (Polymer Laboratories) at a frequency of 1 Hz, with a displacement 0.005 mm along the diameter direction. The values of T_g were read off as the temperatures of the peak of loss modulus.

In this study, the swelling behaviour of the bulk hybrid polymers was investigated by leaving carefully weighted normalized samples of polymers in ethylacetate and water for 3 and 30 days. Then the percentage weight increase of all the samples was determined and the swelling index (I_{sw}) could be calculated according to [9,59]:

$$I_{sw} = (\text{wet weight} - \text{dry weight})/\text{dry weight}$$

The degrees of swelling as a function of the increasing ratio monomer/cluster are reported in Table 4.

Finally the morphology of the coatings was explored by ESEM (Environmental Scanning Electron Microscopy) (Philips XL30 ESEM-TMP).

The Energy Dispersive X-ray Spectra (EDXS) were acquired through the FALCON X-ray detector for preparing chemical composition maps of selected regions of the samples.

UV spectra were acquired on bulk samples by using a Cary 5000 spectrophotometer, in the spectral range 200–500 nm, with a bandwidth of 1 nm and an acquisition time of 0.1 s/step. Nanoindentation was used to determine the mechanical properties of the films using a Nanotest 600 instrument from Micromaterials Ltd with a Berkovich (three-sided pyramidal) diamond indenter. The indentations were performed at maximum load of 3 mN and repeated 10 times on different regions of the sample surface apart 200 μm. The hardness and the elastic recovery of the coatings were determined from the obtained indentation curves as previously described [60].

3. Results and discussion

3.1. Optimisation of the curing time

In order to optimise the time for UV curing of the hybrid coatings, the kinetics of the photopolymerisation in the films was determined by FT-IR spectroscopy. The liquid formulations were coated onto a silicon (100) wafer and the polymerisation process was monitored by recording the intensity variation of the C═C band at 1640 cm^{-1}, with respect to the C═O band (1725 cm^{-1}) adopted as internal standard (data not shown). In particular, the ratios of the areas of the two bands should decrease upon polymerisation, since C═C bond are consumed, whereas the C═O remain unchanged. After each curing steps of 5, 10 and 20 min a FT-IR spectrum was recorded as shown in Fig. 1. The ratio of the peak areas was plotted as a function of time and it was evidenced that for

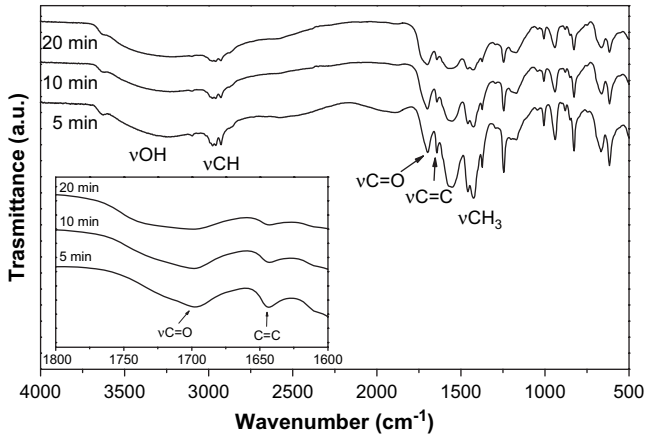

Fig. 1. Normalised IR spectra of Zr4:MMA 1:100 after 5, 10 and 20 min of photopolymerisation.

two samples, characterised by Zr4:MMA molar ratios of 1:50 and 1:100, respectively, a 10 min curing is sufficient to obtain completely polymerised films (strong decrease of C═C bands, which are consumed upon polymerisation). On the basis of these results, the curing time was set at 10 min. Similar results had already been obtained in the case of the copolymerisation of the Zr oxocluster with the methacrylate-functionalised silane [61].

3.2. Surface and in-depth composition of the coatings

The surface composition of two selected film samples (Zr4:MMA 1:100 photoinitiator 4.2 wt%, Zr4:MMA 1:100 photoinitiator 8.4 wt%) was analysed by XPS providing information also on the oxidation state and chemical environment of the species. In the survey of the sample Zr4:MMA 1:100 deposited on polymethylmethacrylate (data not shown), all the species of interest (Zr, O, C) could be detected.

XPS analysis was carried out on different points of the surface of the coating deposited on PMMA and by using different take-off angles (30°, 45° and 60°) to evaluate the lateral and in-depth composition of the samples, at least in the first layers beneath the surface. In this framework, the use of AR-XPS to analyse different depths of the coating was mandatory. In fact, in the case of polymeric-based coatings, ion sputtering can not be applied for in-depth profiling, since it would cause degradation of the organic backbone.

In Table 1, the atomic percentages of the samples Zr4:MMA 1:100 deposited on PMMA taken at two different points and with different take-off angles are reported, which show similar atomic percentages for different analysed points, thus evidencing a good lateral and vertical compositional homogeneity.

Table 1
Atomic percentages and BE values of sample Zr4:MMA 1:100 on polymethylmethacrylate as determined by XPS

Sample	Composition	%O	%Zr	%C	BE Zr3d (eV)	BE O1s (eV)
Zr4_point A	Zr4:MMA 1:100, Init. 4.2 wt% point A	22.1	0.8	77.1	182.8	532.6
Zr4_point B	Zr4:MMA 1:100, Init. 4.2 wt%, point B	25.5	0.7	73.8	183.0	532.2
Zr4_angle 45°	Zr4:MMA 1:100, Init. 4.2 wt%, AR = 45°	22.5	2.3	75.2	182.7	532.2
Zr4_angle 60°	Zr4:MMA 1:100, Init. 4.2 wt%, AR = 60°	22.1	2.5	75.4	182.6	532.2
Zr4_angle 30°	Zr4:MMA 1:100, Init. 4.2 wt%, AR = 30°	21.4	2.2	76.4	183.2	532.4
Zr4_point_A	Zr4:MMA 1:100, Init. 8.4 wt%, point A	25.4	1.9	72.7	183.0	532.0
Zr4_point_A′	Zr4 MMA 1:100, Init. 8.4 wt%, point A′ (after X-rays irradiation)	25.4	1.8	72.8	183.6	533.2

As far as the chemical state of the species is concerned, the binding energies (BE) of the oxygen O1s region, once corrected for charging effects, are in the range 530.9–531.3 eV, values typical of oxygen in polyacrylates [51,52]. The BE of Zr3d region ranges in the interval 182.6–183.0 eV, which are values typical of zirconium in an oxidic environment. This is reasonable since the zirconium in the cluster is surrounded by the oxygen bonds of the Zr–O–Zr bridges and by the oxygen of the chelating and bridging carboxylates. The binding energy values of the species in the hybrid polymers are comparable with those measured for the pure cluster, but this can not be assumed as a proof that the cluster structure was retained, since XPS only provides information on chemical state (e.g. oxidation state) and on the environment of an atom, as well as on the chemical nature (e.g. electronegativity, etc.) of its first neighbours. At this regard, as described in the following, EXAFS is providing more information.

In order to check for degradation of the polymer matrix possibly induced by X-ray irradiation [47], the samples were analysed twice under the same conditions but with a delay time of 60 min. The two C1s spectra acquired immediately and after 60 min (data not shown) are practically identical.

Furthermore also the atomic percentages of the elements are identical before and after X-ray irradiation (see Table 1) and the C1s region does not show any broadening or further component with respect to the sample analysed before irradiation, which would suggest the presence of different chemical environments caused by the degradation of the organic polymer. These findings were also confirmed by IR spectra (data not shown).

As it can be seen, as mentioned above, the detected atomic percentages are very similar on two different points spaced by about 2 cm of the surface, thus indicating a good lateral homogeneity of the samples. Also the atomic percentages recorded at different depths are very similar, thus indicating that the zirconium oxocluster is evenly distributed along the layer. This latter finding was confirmed by SIMS analyses *(vide infra)*, which were carried out on two different samples, Zr4:MMA 1:100 and Zr4:MMA 1:50 deposited on PMMA.

3.3. Surface morphology and coating thickness

The films are homogeneous, transparent and well adherent to the substrate, despite of the nature of the underlying material, the only exception being the depositions on aluminum. Nanoindentation tests were carried out on the coatings on different substrates (data not shown) to study their surface mechanical properties. In particular, in order to get a more representative view, 10 different analyses on 10 different points spaced about 200 μm were performed at a maximum load of 3 mN.

By plotting the different curves load vs. displacement acquired for each sample (data not shown), a good overlapping of the different experimental curves was evidenced, thus showing identical mechanical properties at different points of the analysed surfaces. This holds for all substrates, except than for aluminum, for which the poorer result can be traced back to the very scarce adhesion between the aluminum substrate and the polymer-based coating. Conversely, the best overlap (i.e. the most uniform mechanical properties) were achieved for the coatings deposited on polymethylmethacrylate that show the higher hardness and elastic recovery values (0.43 ± 0.04 GPa and 20% respectively). In this case, the identical chemical nature of substrate was proven to play a pivotal role in enhancing the lateral homogeneity of the coatings. Analogously, the presence of the zirconium oxocluster, increasing the cross-linking of the polymer, was also strongly

contributing to the uniformity of the coatings. Similar coatings prepared without cluster were in fact characterised by very poor homogeneity and scarce adhesion. On the contrary, the relative amounts of cluster and of the photoinitiator were not proved to remarkably influence the quality of the coatings.

Furthermore, the coatings are stable and still adherent also after several weeks. As far as the adhesion is concerned, previous experiments carried out on similar samples, have shown that the best results, in terms of adhesion to the substrate, evaluated by home-made pull-off tests, were obtained in the case of the higher compatibility between substrate and film, i.e. in the case of polyethylene and PMMA as substrates, in agreement with nanoindentation data.

The film thickness was determined by considering the Zr signal (thickness at full width at half maximum). The error in the thickness determination is strongly influenced by the surface roughness. In the produced films, the thicknesses range from 2 to 10 μm according to the deposition parameters. The coatings obtained with a ratio 1:100 show a uniform distribution of Zr across the film deposited on both the PMMA substrate and the stainless steel, as shown in Fig. 2. The interface film–substrate is quite sharp (close to 200 nm thick) for the film deposited on PMMA substrate. This finding is mainly due to the different surface roughness of these two substrates. Moreover a carbon segregation peak could be observed in the PMMA substrate, while in the stainless steel one it is not detectable.

The coating with 1:50 ratio deposited on PMMA substrate, instead, shows a strong variation in the element distribution with a broadened interface (the film roughness is close to 1–1.5 μm depending on the analysed point).

As already discussed above, regardless of the substrate on which they were deposited, the obtained coatings are homogeneous and transparent. This was also confirmed by the optical microscopy investigations. To get a better insight on the surface morphology of the hybrid samples, Zr4:MMA 1:100 deposited on polymethylmethacrylate, aluminium and stainless steel, respectively, they were investigated by ESEM. In the ESEM of sample Zr4:MMA 1:100 on aluminium (data not shown), the surface appears homogeneous and crack-free on the 20 μm lateral scale. However, fractures appear on a larger scale, which can be ascribed to a shrinkage of the hybrid during UV curing, which in turn decreases the adhesion of the coating to the underlying substrate.

As discussed in the following Section 3.5, the oxocluster induces a shrinkage of the polymer matrix and a slight greater glassy behaviour, which leads to cracks formation.

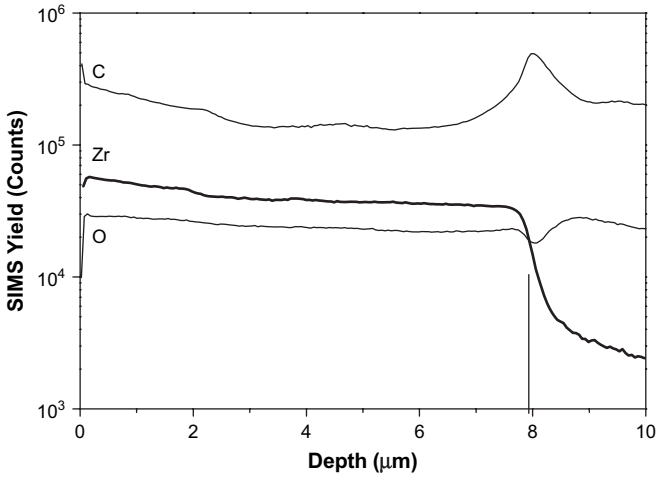

Fig. 2. SIMS depth profile of sample Zr4:MMA 1:100 on polymethylmethacrylate.

3.4. X-ray absorption spectroscopy

Since the properties of hybrid materials depend also on the interaction at the interphase and, in particular, on molecular level intermixing through the formation of strong chemical bonds among the inorganic and organic building blocks, the analysis of the local environment of Zr and the determination of the actual bond lengths are extremely useful in order to understand the process mechanisms and to determine the optimized preparation conditions. To this aim, in order to investigate the chemical environment around the zirconium ions, the chemical bond lengths, and to study the effect of thermal treatments and swelling in water on the prepared coatings, seven bulk samples, listed in Table 2, were analysed by X-ray absorption spectroscopy (XAS), yielding coordination numbers and bond distances.

Fig. 3 shows the XANES spectra of bulk samples of Zr4 in polymethylmethacrylate matrix 1:50 produced by 4.2 wt% photoinitiator, after thermal treatment in the range 100–250 °C, and after swelling in H_2O. For comparison the spectra of Zr4:MMA 1:100 without post-treatment is also shown.

Rather subtle features of the absorption edges are more significant in the derivative spectra, which are also shown. All samples show a shoulder in the XANES region before the edge jump (marked with an oval in Fig. 3, bottom left), which is indicative of a distortion from centrosymmetry [62]. This shoulder is also significant in the derivative spectra, and its corresponding feature is enlarged in Fig. 3 (bottom right). Since the intensity of this feature is comparable for all samples, their degree of distortion should be also quite similar.

The shape of the first resonance after the edge jump (white line) itself can be used to distinguish different coordination geometries at the zirconium center. Octahedral coordination sites show a splitting of the white line (s → p-transition), while a broad single band is observed for seven- and eight-fold coordination sites [63,64]. According to Fig. 3, the samples can be divided into two groups by using this criterion. In the first derivative, the splitting becomes more pronounced with a signal at around 18.025 keV.

Four samples (Zr4:MMA 1:100 without thermal treatment, Zr4:MMA 1:50 treated at 200 and 250 °C, and after swelling in water) show an obvious signal at 18.025 keV, from which an average oxygen coordination number of around six can be deduced. Nevertheless the intensity of this signal is significantly higher in the last two samples and the geometry of the 6-fold coordination should be different in comparison to the first two. This result is further confirmed by the EXAFS analyses in the second part of this Section. Since the samples Zr4:MMA 1:50 without thermal treatment, and treated at 100 and 150 °C do not show such a signal at 18.025 keV, a 7- or 8-fold oxygen coordination of similar geometry is expected in these samples.

It is noteworthy that the isosbestic points in the absorption and derivative spectra of the Zr4:MMA 1:50 row (highlighted with rectangles) prove that the zirconium content of the different measured samples were the same and the observed spectral changes are only due to a change in the coordination details of the samples, i.e. they are not caused by changes in the zirconium concentration. The different Zr4:MMA ratio of the Zr4:MMA 1:100 sample is therefore the reason for which it does not cross the isosbestic points.

As far as the analysis of the EXAFS part of the absorption spectra is concerned, the results of fitting the experimental spectra with theoretical models are reported in Table 2. The according experimental $k^3 \cdot \chi(k)$ spectra and their corresponding Fourier transformed functions are shown in Fig. 4.

All samples show an oxidic nearest neighbour coordination, in agreement with the XPS results. As it can be seen from the table, the obtained total oxygen coordination numbers agree very well with

Table 2
Numeric results from fitting the experimental EXAFS spectra with theoretical models

Sample	Abs–Bs[a]	N^b (Bs)	R^c (Å)	σ^d (Å)	*R*-factor	E_f (eV)
$Zr_4O_2(OMc)_{12}$ (XRD)	Zr–O	4.5	2.14			
	Zr–O	3.0	2.23			
	Zr–Zr	2.5	3.59			
Zr4:MMA 1:100	Zr–O	4.9 ± 0.3	2.09 ± 0.02	0.067 ± 0.004	17.22	9.22
	Zr–O	1.7 ± 0.1	2.23 ± 0.02	0.032 ± 0.002		
	Zr–C	4.9 ± 1.0	2.80 ± 0.03	0.112 ± 0.022		
	Zr–Zr	1.1 ± 0.2	3.33 ± 0.03	0.102 ± 0.020		
Zr4:MMA 1:50	Zr–O	1.5 ± 0.1	2.07 ± 0.02	0.059 ± 0.003	21.18	8.97
	Zr–O	5.9 ± 0.3	2.19 ± 0.02	0.092 ± 0.005		
	Zr–C	4.4 ± 0.9	2.79 ± 0.03	0.112 ± 0.022		
Zr4:MMA 1:50 100 °C	Zr–O	1.2 ± 0.1	2.05 ± 0.02	0.055 ± 0.003	17.88	7.85
	Zr–O	6.2 ± 0.3	2.19 ± 0.02	0.087 ± 0.005		
	Zr–C	3.0 ± 0.6	2.81 ± 0.03	0.112 ± 0.022		
	Zr–Zr	0.2 ± 0.0	3.50 ± 0.04	0.022 ± 0.004		
Zr4:MMA 1:50 150 °C	Zr–O	1.6 ± 0.1	2.07 ± 0.02	0.055 ± 0.003	29.96	7.25
	Zr–O	5.6 ± 0.3	2.20 ± 0.02	0.087 ± 0.005		
	Zr–C	2.7 ± 0.6	2.80 ± 0.03	0.112 ± 0.022		
	Zr–Zr	0.2 ± 0.0	3.51 ± 0.04	0.022 ± 0.004		
Zr4:MMA 1:50 200 °C	Zr–O	2.9 ± 0.1	2.05 ± 0.02	0.032 ± 0.002	24.25	9.48
	Zr–O	3.5 ± 0.2	2.20 ± 0.02	0.032 ± 0.002		
	Zr–C	4.3 ± 0.9	2.78 ± 0.03	0.097 ± 0.020		
	Zr–Zr	0.2 ± 0.0	3.52 ± 0.04	0.059 ± 0.012		
Zr4:MMA 1:50 250 °C	Zr–O	5.9 ± 0.3	2.10 ± 0.02	0.081 ± 0.004	13.35	8.60
	Zr–C	5.1 ± 1.0	2.72 ± 0.03	0.112 ± 0.022		
	Zr–Zr	0.6 ± 0.1	3.34 ± 0.04	0.063 ± 0.013		
Zr4:MMA 1:50 after swelling	Zr–O	6.5 ± 0.3	2.08 ± 0.02	0.087 ± 0.005	16.16	13.15
	Zr–C	6.8 ± 1.4	2.69 ± 0.03	0.112 ± 0.022		
	Zr–Zr	0.6 ± 0.1	3.32 ± 0.04	0.112 ± 0.022		

[a] Abs = X-ray absorbing atom, Bs = backscatterer.
[b] Coordination number.
[c] Interatomic distance Abs–Bs.
[d] Debye–Waller like factor.

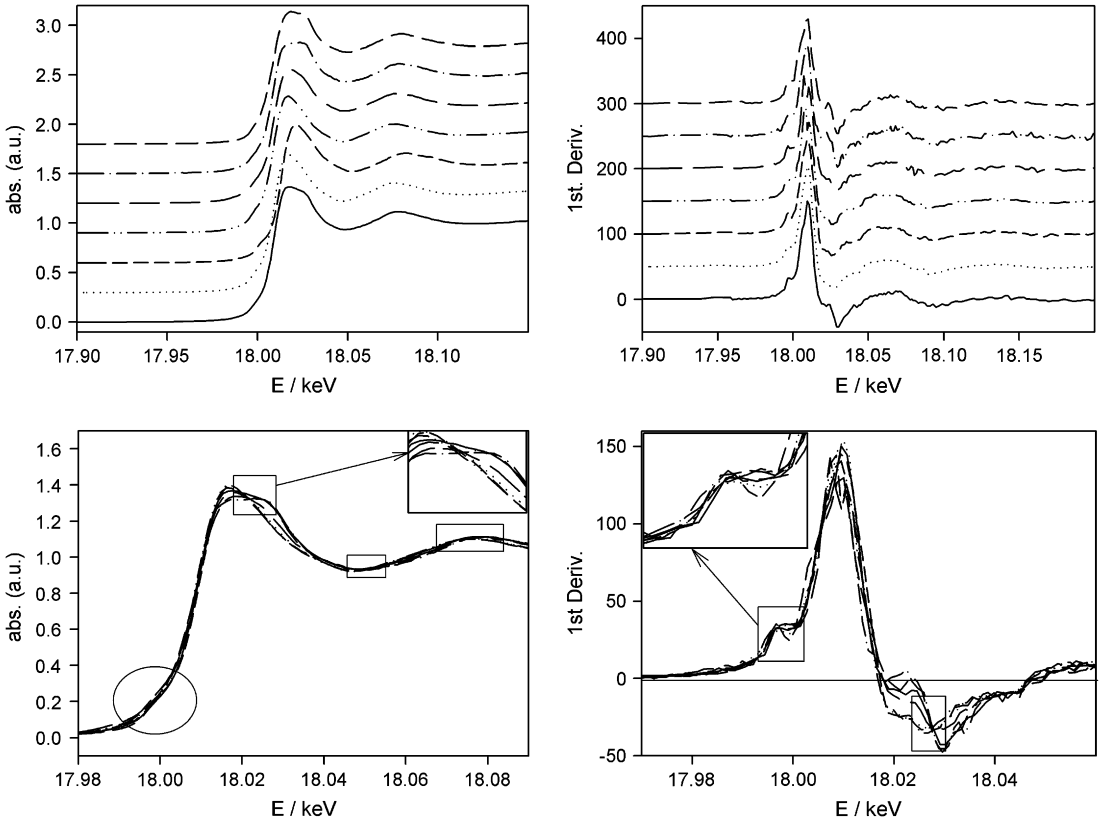

Fig. 3. X-ray absorption spectra (left) of samples Zr4:MMA 1:100 without thermal treatment (solid line), Zr4:MMA 1:50 without thermal treatment (dotted line), Zr4:MMA 1:50 with thermal treatment at 100 °C (short dashed line), at 150 °C (double dotted dashed line), at 200 °C (long dashed line), at 250 °C (dotted dashed line) and without thermal treatment with swelling in water (medium dashed line). The differential spectra are shown on the right. On top the spectra were shifted on the ordinate for better individual representation. Marked areas and enlarged features are explained in the text.

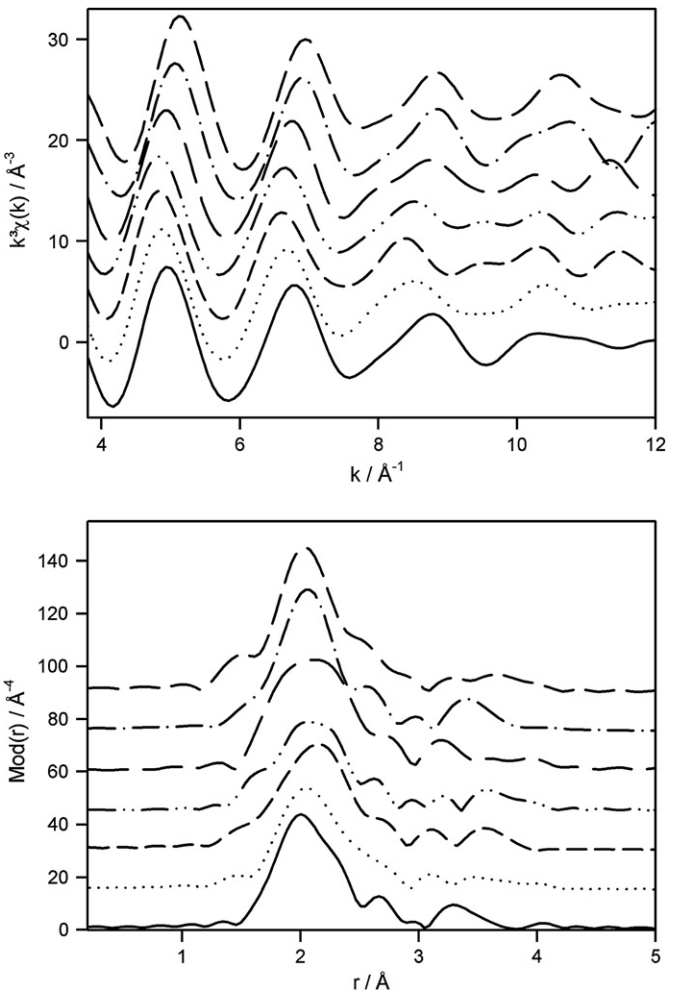

Fig. 4. Fourier filtered $k^3 \cdot \chi(k)$ functions (top) of samples Zr4:MMA 1:100 without thermal treatment (solid line), Zr4:MMA 1:50 without thermal treatment (dotted line), Zr4:MMA 1:50 with thermal treatment at 100 °C (short dashed line), at 150 °C (double dotted dashed line), at 200 °C (long dashed line), at 250 °C (dotted dashed line) and without thermal treatment with swelling in water (medium dashed line) and their corresponding back transformed functions (bottom). For clarity, the spectra were shifted on the ordinate.

the results from the XANES analysis. Nevertheless, the number of subshells, and the distribution of atoms in these shells suggest a fine sub-division of the samples characterised into three groups. As a matter of fact, the samples Zr4:MMA 1:50 without thermal treatment, and the same sample treated at 100 and 150 °C show two separate oxygen shells of average 1.4 and 5.9 atoms at a distance of around 2.06 and 2.19 Å, thus leading to a total Zr–O coordination number of around 7.3. This means that the chemical environment and the structure of the inorganic building block, present in the starting material, is retained also after annealing up to 150 °C. In contrast, thermal treatment at higher temperature (>150 °C) induces some change: after treatment at 200 °C, in fact, still two oxygen shells can be found in the samples Zr4:MMA 1:50, although the oxygen coordination number is reduced to 6.5. A similar chemical environment was also detected for Zr4:MMA 1:100 without thermal treatment, although the distribution of these atoms over the two shells is different for both samples. The third group includes the sample Zr4:MMA 1:50 after treatment at 250 °C and after swelling. Although the total oxygen coordination number is similar to Zr4:MMA 1:50 treated at 200 °C, which is in accordance to the XANES interpretation, only one oxygen shell with 5.9 and 6.5 atoms, respectively, could be adjusted. This can be ascribed to a further degradation of the initial structure of the inorganic building block upon these harsh handlings.

An overview of all the shells and the contained number of atoms is given in Fig. 5 top, while in the bottom of this figure, the total number of oxygen backscatterers is correlated to the white line shape. The results agree well with data previously reported in literature [63,64]. The changes in the oxygen shell induced by increasing temperature and also after the swelling in water indicate a rearrangement process of the ligands and a change in the aggregation degree, which will be considered in the following discussion of the zirconium shells. Since the sample Zr4:MMA 1:100 without thermal treatment is the only one with this particular cluster to monomer ratio, it will be discussed first.

Although the metal concentration in Zr4:MMA 1:100 is less than that in the other samples, it shows the highest aggregation degree of the metal centers, since approximately one Zr neighbour is found, which can be interpreted by the presence of dimers. Also, it is only this sample, for which a remaining structural relation to the initial Zr4-cluster can be observed by comparison with the XRD-data of the crystalline cluster in Table 2 [14]. But the significantly reduced coordination numbers indicate a large degree of degradation of the Zr4-cluster. This is supported by the reduced distances in the first oxygen and zirconium shell, which are enabled by an overall reduction of the coordinating atoms.

In contrast, the sample Zr4:MMA 1:50, for which twice the Zr4 concentration of Zr4:MMA 1:100 was used, shows no Zr–Zr neighbours at all. Despite the increased metal content, no dimeric but only monomeric zirconium centers can thus be found, which exhibit also a completely different oxygen coordination than the dimers in Zr4:MMA 1:100. It can be therefore concluded that the cluster to monomer ratio is strongly affecting the formed structures.

In summary the XANES and EXAFS analyses show that, in the experimental conditions used, the cluster undergoes a certain degree of degradation, which can be possibly ascribed to the nonanaerobic conditions used during photopolymerisation/deposition of the layers.

The effect of temperature on the structure of the inorganic building blocks inside the materials, already evidenced by XANES results, can be further specified by EXAFS data analysis. With increasing temperature a maximum of 20% dimers can be deduced from the Zr–Zr coordination number of 0.2. The distance of the zirconium shell is 0.2 Å larger than for Zr4:MMA 1:100, which can be assigned to a reapproachment of the zirconium centers, which were probably taken separated by the decomposition of the Zr4-cluster during polymerisation. At 200 °C significant changes in the oxygen shells can also be observed in the Fourier transformation, where both shells are almost equally populated, while the Zr–Zr coordination remains constant. The onset of burning of the hydrocarbon residues is suggested as possible explanation, since it would allow rearrangements in the oxygen coordination. This is supported by the results of the sample, which was treated at 250 °C. The increased Zr–Zr coordination number of 0.6, from which a fraction of ~50% dimers can be deduced, can be explained by removal of bulky organic groups that allow the zirconia centers to reduce their distance. Since also only a single oxygen shell is present at this temperature, the formation of pre-ZrO_2 structures can be concluded. The same is found for the samples treated with water. Here, hydrolysis and condensation processes can cause the formation of pre-ZrO_2 structures. The reduction of the Zr–Zr distance is supporting this conclusion, since it can also be found for the first Zr–Zr shell in monoclinic ZrO_2 [65], as well as in zirconia–silica xerogels with low zirconium content [66]. It should be stressed again, however that only pre-ZrO_2 structures can be formed, since the presence of carbon excludes purely oxidic structures. Although the increased number of carbon atoms at higher treatment temperatures is somewhat contradictory, it should be noted that the properties of carbon as light backscatterer,

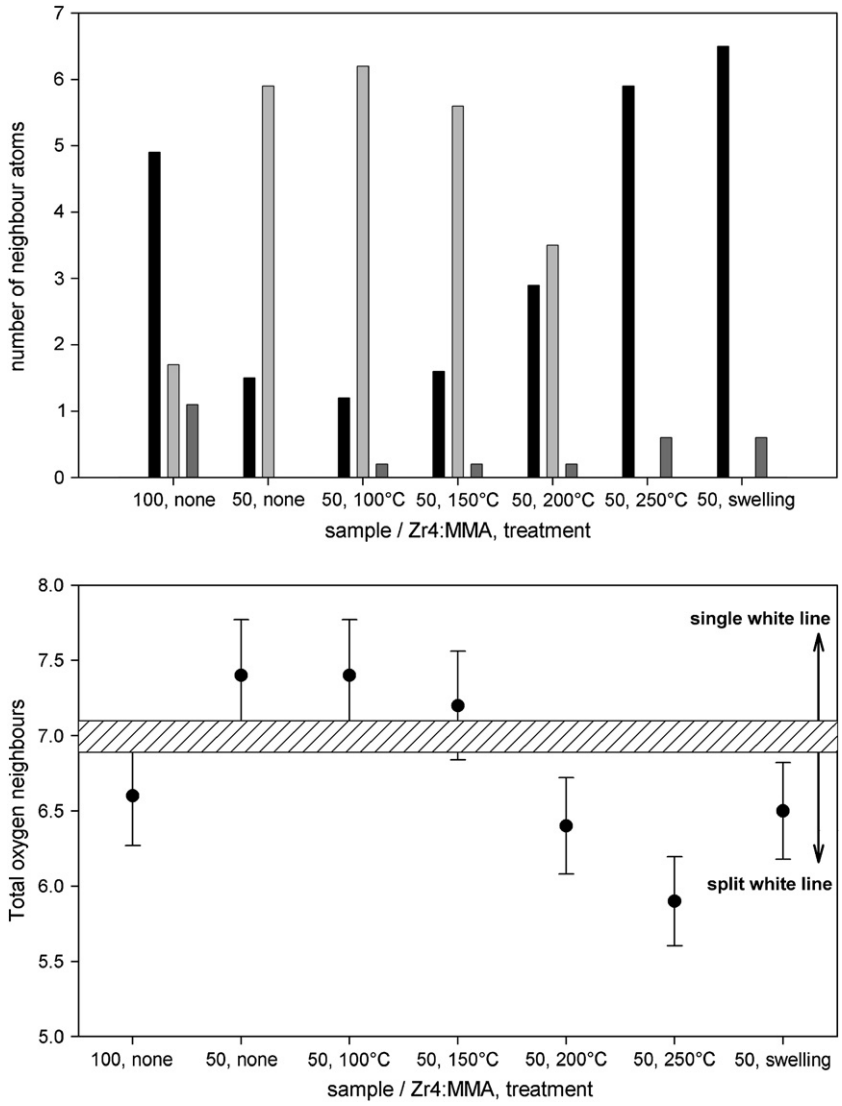

Fig. 5. Graphical overview of the fit results (top): first oxygen shell at 2.05–2.10 Å (black bars), second oxygen shell at around 2.20 Å (light grey bars) and zirconium shell (dark grey bars). The total oxygen coordination number of all samples compared to the white line shape in the bottom.

limit the reliability of the obtained *C*-coordination numbers: the Zr–C distances are, instead, in accordance with that found for similar systems [64].

3.5. Thermal investigation and dynamic-mechanical investigation

Although the properties of thin polymer films are expected to be different from those of the bulk state (the T_g value of the polymer in form of thin film is greater or lower than the corresponding bulk value, according to the higher or lower interfacial energy, respectively), we used bulk samples (prepared by using the same formulations used for the coatings) for studying the effect of oxoclusters' incorporation.

In particular, in order to evaluate the effect of the cluster incorporation on the thermal behaviour of the UV-photopolymerised materials, thermal analyses were carried out on different bulk materials. As far as the thermal stability is concerned, interesting information were gained by TGA. In Fig. 6 the TGA data of neat PMMA and of three hybrid samples are plotted. Whereas PMMA shows the main mass loss with an onset temperature of thermal degradation at 240 °C, the thermal degradation of the hybrid materials reinforced with the cluster is shifted of about 110 °C. Among the different hybrids, no noticeable differences were pointed out. The residual weights are in agreement with those calculated by assuming a complete conversion of the hybrid materials into zirconium dioxide.

In Fig. 7 the heat flow curves vs. temperature of neat PMMA (a) and hybrid Zr4:MMA 1:200 (b) are shown. The curve of PMMA shows a continuous release of volatile species from 200 up to 400 °C due to depolymerisation, which is reported to occur at 330 °C for pristine PMMA [14,59,67,69]. The hybrid material evidences a first mass loss (in thermal range 200–300 °C), which corresponds to evaporation of low molecular weight species, followed by a second larger mass loss at 385 °C, corresponding to the depolymerisation of the organic polymeric chains. At higher temperature, about 430 °C, a third mass loss was observed and attributed to the combustion of the remaining organic parts, which leaves only ZrO_2 as inorganic residue. On account of these results, it can be stated that the hybrid materials display a higher thermal stability with respect to the pristine PMMA, as already reported for similar hybrid systems prepared by thermal polymerisation [14,25,38,39].

In order to analyse the mechanical behaviour of the hybrid samples and to compare it with that of neat PMMA, dynamic-mechanical tests were performed on different bulk samples in the

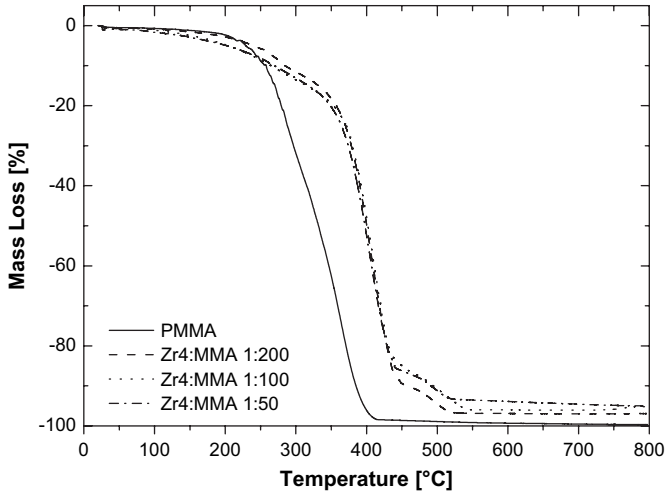

Fig. 6. Thermogravimetrical curves of the hybrid samples and of PMMA acquired in air.

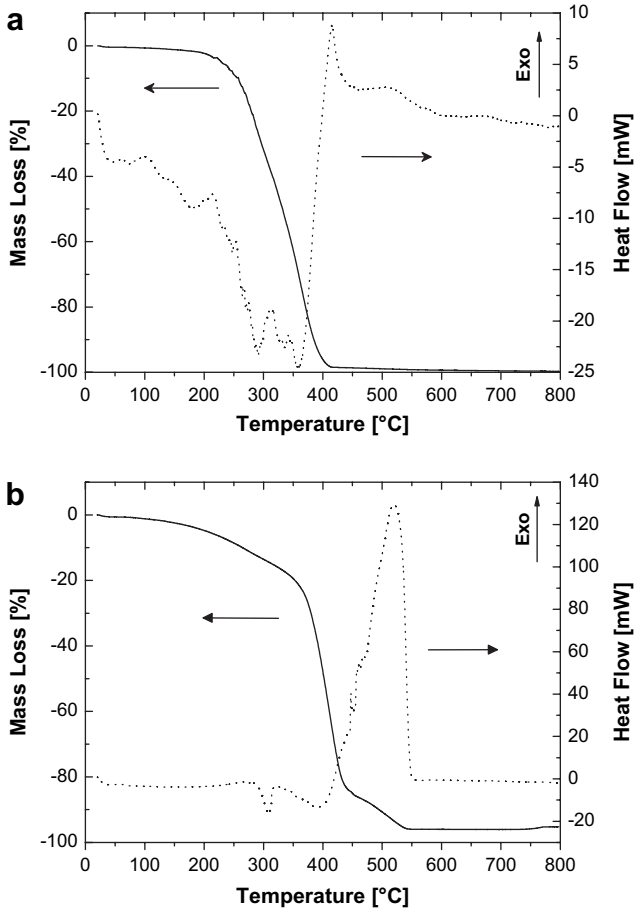

Fig. 7. TG and heat flow curves of neat PMMA (a) and of Zr4:MMA 1:200 (b).

range 25–200 °C, i.e. before the beginning of depolymerisation, reported to occur at 330 °C [67]. Actually, it was assessed that the thermal behaviour of UV-photopolymerized PMMA-based material depends on the preparation conditions, especially on sample thickness and curing time.

In fact, DSC of neat PMMA in the range of 25–200 °C, (data not shown), evidences a lower glass transiton (85 °C), followed by a higher one at 104 ± 1 °C. This suggests that two fractions are present, probably due to two different photopolymerisation kinetics, in the inner and outer parts of the bulk polymer, which can in turn be ascribed to the different penetration depth of the UV light in the bulk sample. Actually, UV spectra acquired on the bulk sample show a noteworthy absorption of UV from the sample itself, which in turn hinders a complete polymerisation of the deeper regions. Accordingly, this phenomenon was instead not observed in the thin films, where a complete polymerisation occurred along the whole thickness, as also shown by IR data. As a matter of fact, bulk pristine PMMA foams during analysis, whereas in the second scan only the highest temperature glass transition is present, according to the previous hypothesis. The presence of a fraction having a lower T_g value, though less pronounced, was also observed in the DSC curves of hybrid samples. As a consequence, to complete the polymerisation, all the samples, before DMTA analysis, underwent a thermal treatment at 80 °C.

In Table 3, the T_g and storage moduli before and after glass transition of all the bulk samples are reported.

Whereas neat PMMA was degradated after the first scan, all the hybrid bulk samples underwent repeated DMTA scans and they show an increase in the T_g. The evidenced trend is that the storage moduli at 30 °C of the hybrid materials are slightly greater than that of neat PMMA, resulting to be 230 MPa. Furthermore, these values become remarkably higher at temperatures higher than the T_g. It should be moreover highlighted that also the high temperature behaviour is noticeably different going from the pure viscous flow of PMMA to the rubbery plateau of the hybrids polymers. This is a clear indication of the cross-linking induced by the zirconium oxocluster, which leads to a highly interconnected network after thermal treatment. Furthermore, it has to be pointed out that the observed improvement in the thermal stability could also be ascribed by the role played by the cluster as inorganic filler. It has in fact already pointed out [39] that the improvement in the thermal stability can be ascribed both to the crosslinking of the cluster and its effect as filler.

The cross-linking increase (C) is a key factor in order to evaluate the effect of the oxocluster concentration as well as the homogeneity of their distribution. This parameter can be defined as:

$$C = \frac{G'_a}{G'_b - G'_a}$$

where G'_b and G'_a denote the storage moduli before and after the glass transition, respectively, calculated at the same temperature [68–70]. The G'_b, G'_a and C values for all the samples and after repeated scans are reported in Table 3. It can be observed that C increases by increasing the number of scans, whereas the correlation with the oxocluster concentration is not really clear. Indeed, C shows the highest values for Zr4:MMA 1:100.

These results are also in agreement with those of the swelling experiments in water and ethylacetate, which are reported in Table 4.

Indeed, the derived hybrids absorb slightly more solvent than the neat polymer after 3 days. However, taking into account the swelling index, it was observed that this swelling index that is the amount of retained solvent, is doubled after 30 days. Accordingly, PMMA, being a linear polymer, is soluble in ethylacetate, whereas the hybrids swell. This behaviour is in agreement with that observed for similar hybrid materials produced by thermal polymerisation [14,29] and has been ascribed to the cross-linking induced by the organically modified oxocluster. As a consequence of the solvent uptake, the hybrid materials increase mass, volume and become rubbery. Moreover, in both solvents, the Zr4:MMA 1:100 sample shows a lower swelling degree after longer times. To explain this finding, the density could be taken into account. Indeed this sample shows the highest value of density, higher than PMMA, as the result of a higher cross-linking. Although in previous studies

Table 3
T_g, G' at 30 and 140 °C, C of PMMA, Zr4:MMA 1:200, Zr4:MMA 1:100 and Zr4:MMA 1:50

	T_g [°C]*	G'_b (30 °C) (MPa)	G'_a (140 °C) (MPa)	C (defined in the text)
PMMA	104.0	230	0.0012	0.00053
Zr:MMA 1:200				
1	94.5	320	1.20	0.38
2	92.9	530	1.40	0.42
3	104.8	390	2.20	0.57
4	102.4	360	2.20	0.63
5	105.5	590	3.20	0.54
6	108.3	540	3.40	0.64
7	106.1	340	3.60	1.08
8	107.1	330	4.00	1.23
Zr:MMA 1:100				
1	89.4	380	6.20	1.69
2	85.8	540	7.20	1.35
3	95.4	500	9.20	1.86
4	97.3	330	10.00	3.18
5	102.9	370	13.00	3.60
6	104.7	290	14.00	4.88
7	106.9	410	16.00	4.10
8	104.8	210	12.00	6.21
Zr:MMA 1:50				
1	91.8	590	0.99	0.17
2	97.4	320	0.56	0.18
3	99.7	570	0.32	0.39
4	102.2	470	2.20	0.47
5	104.0	520	2.80	0.55
6	104.7	630	3.00	0.48
7	107.8	430	3.30	0.77
8	107.7	390	3.40	0.87

* The glass transition temperature (T_g) is defined as the maximum of the loss modulus curve.

Table 4
Density of PMMA, Zr4:MMA 1:200, Zr4:MMA 1:100, Zr4:MMA 1:50 and swelling index of the same samples, measured after 3 and 30 days

	%H_2O	%H_2O	%Ethylacetate	%Ethylacetate	Density [g/cm^3]
	3 days	30 days	3 days	30 days	
PMMA	0.65	1.65	Soluble	–	1.060
Zr:MMA 1:200	1.22	2.51	147	188	1.183
Zr:MMA 1:100	1.42	2.16	64	80	1.199
Zr:MMA 1:50	3.00	2.45	51	202	1.190

it has been proven that the lower the oxocluster concentration, the lower the cross-linking is [14,29], it can in this case be assumed that, in the presence of high concentration of oxoclusters, steric hindrance of the clusters themselves occurs, which in turn leads to a lower cross-linking.

The glass transition temperature (T_g) is defined as the maximum of the loss modulus curve, and the experimental values are reported in Table 3. During the first scan, the T_g of the hybrid polymers is lower than that of neat PMMA. Accordingly, the oxoclusters induce a plasticizing effect because the distance among the methacrylate polymeric chains is greater. The bulky oxocluster units force the chains apart over their whole length, thus creating permanent voids. The oxocluster behaves like a spacer between organic chains into the polymer, and, consequently, the mesh of the network increases: the chain motion starts at lower temperature. However, when temperature increases the presence of oxoclusters avoids the sliding of polymeric chains, thus determining a great increase of G'_b (Table 3).

In Fig. 8, the tan δ vs. temperature of all the samples is reported, where temperatures of the maxima of the curves are observed to increase with Zr4 concentration, whereas the intensities decrease.

This is consistent with the hypothesis that the oxoclusters hinder the segmental motions and the viscous flow of the

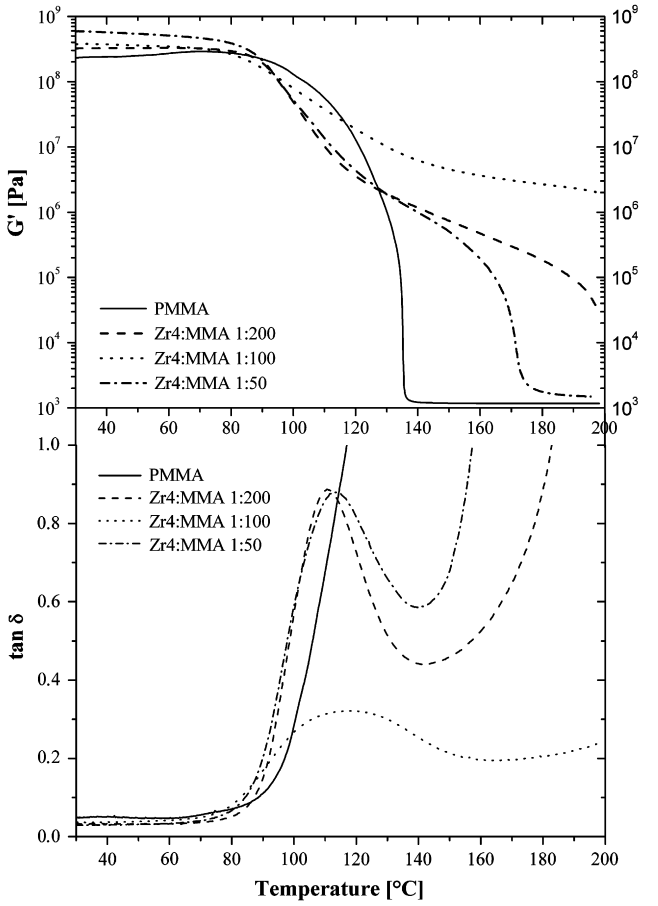

Fig. 8. Plot of G' (above) and tan δ (below) curves vs. temperature of all the samples.

polymeric chains at high temperature (and in organic solvent) (Table 3). Furthermore, the cross-linking, T_g and the maximum of tan δ, which are low after photopolymerisation, increase with the thermal curing; which induces a higher cross-linking of the whole structure, supported by the presence of the oxoclusters.

Meanwhile, the material gets a stable configuration, which maximizes the density and the polymer grafting. In Fig. 9, the size and the mass loss for each scan are reported: both decrease with number of scans, and the slope of the curve decreases too, thus suggesting that the material shrinks attaining a stable configuration and density.

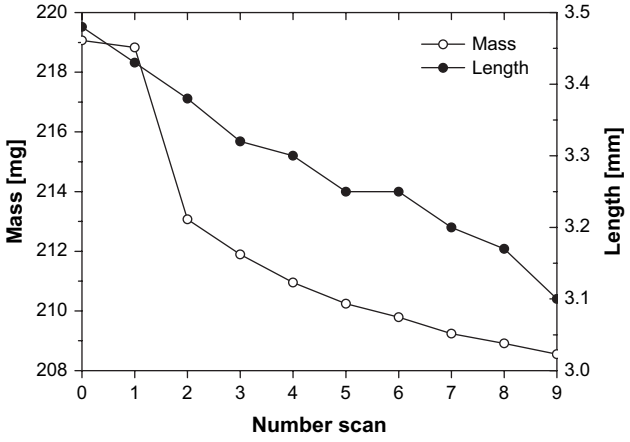

Fig. 9. Mass and size change of Zr4:MMA 1:100 sample after each DMTA scan.

Actually, the UV–vis absorption spectrum of one of the cylindrical hybrid samples (Zr4:MMA 1:100) shows a noticeable absorption, thus evidencing that the sample itself absorbs a relevant amount of the radiation, thus explaining the observed incomplete curing. How and to which extent the oxocluster amount affects the final properties is one of the aspect which results more difficult to be explained. Indeed, if it was evidenced that within a 1 mol% of oxocluster (Zr4: MMA 1:100), the main effect is the increase of T_g and cross-linking, whereas the effect is less clear when the amount of the oxocluster is higher than 1 mol%. It was evidenced by Schubert et al. [68] that at higher concentration the oxoclusters are randomly aggregated, forming clusters of clusters ranging from about 5 to 100 nm.

Although this effect was not taken into account in this study, the aggregation of clusters is surely present also in our samples, thus affecting the final properties to an extent not exactly neither experimentally evaluable.

4. Conclusions

UV-photopolymerisation (in the case of coatings carried out during simultaneous spray-coating deposition) was successfully applied to prepare zirconium-oxoclusters reinforced inorganic–organic hybrid materials, both as bulk specimens and as coatings on different substrates.

The composition of the films was analysed by XPS and SIMS, evidencing a good lateral and vertical distribution of the zirconium cluster in the materials. X-ray absorption spectroscopy was successfully applied to elucidate the local structure around the zirconium centers. A combination of XANES and EXAFS analysis provided a detailed picture of the oxygen and zirconium coordination, by which the effect of different post-synthesis treatments could be identified.

The thermal and mechanical behaviour of the bulk hybrid samples with respect to neat PMMA was elucidated by the results of Dynamical Mechanical Thermal Analysis. Indeed, the hybrid samples behave as a cross-linked polymer, showing a quite remarkable value of storage modulus after glass transition, which allows the specimens to retain their shape, whereas the neat polymer flows during glass transition. The cross-linking degree increases with thermal treatments. However, due to the presence of the oxocluster, the complete and homogeneous polymerisation could not be completely attained and this can affect the results and the recorded values of T_g. The oxocluster restrains the movement of the polymeric chains and extends the distance among adjacent polymeric chains. As a consequence, the free volume of the hybrid samples is higher than that of the neat polymer, regardless of the oxocluster content. On the contrary, the highest increase of cross-linking (calculated as the ratio between the difference of storage modulus before and after T_g and the storage modulus before T_g) was shown from the sample having a medium oxocluster content.

The thermal cycling affords materials which are highly reliable from a thermal point of view, and which retain their features without any further shape and mass loss. According to these results, it can be concluded that the oxocluster noticeably improves the thermal properties of the polymer, backbone which retains transparencies, shape and size after glass transition temperature up to 300 °C.

Furthermore, for the hybrid materials, a gradual improvement of the mechanical properties was observed with increasing number of scans, which can be ascribed to an increasing curing of the polymer.

Acknowledgments

BM08 Gilda at European Syncrothron Radiation Facility (ESRF), Grenoble (France), is gratefully acknowledged for the provision of synchrotron radiation for EXAFS measurements. GILDA is a project jointly financed by CNR and INFN, Italy. Dr. Francesco D'Acapito is gratefully acknowledged for the helpful technical and scientific support during XAS measurements in the framework of proposal number 08-01-768. The CNR, the University of Padova, Italy, INSTM, the University of Trento, Italy and the Deutsche Forschungsgemeinschaft (DFG), Germany, are acknowledged for the financial support. Ciba Specialty Chemicals, Basel, Schweiz, is acknowledged for the kind supply of photoinitiators. F. Graziola thanks the University of Trento (Italy) for a research scholarship. The authors thank Dr. G. Bottaro for UV–vis absorption spectra and Prof. L. Fambri and Prof. E. Tondello for the helpful discussion. Finally, the authors would like to acknowledge Mr. Lorenzo Dainese, Mr. Stefano Mercanzin (Workshop of the Dipartimento di Scienze Chimiche, University of Padova) and Mr. Antonio Ravazzolo (CNR-ISTM) for the precious helpful technical support and in particular Mr. Lorenzo Dainese for the realization of a home-made dry-box (*Kasse*, University of Padova, 2008) for simultaneous spray-coating deposition and UV curing of hybrid coatings under controlled atmosphere.

References

[1] Sanchez C, Julian B, Belleville P, Popall M. J Mater Chem 2005;15:3559.
[2] Sanchez C, Romero PG, editors. Functional hybrid materials. Weinheim: Wiley-VCH; 2004.
[3] Kickelbick G, editor. Hybrid materials, synthesis, characterization and applications. Weinheim: Wiley VCH; 2007.
[4] Ochi M, Takahashi R, Tenanchi A. Polymer 2001;42:5151.
[5] Tong Y, Yu Y, Ding J. J Appl Polym Sci 2002;83:1810.
[6] Sanchez C, Soler Illia GJ, Ribot F, Lalot T, Mayer CR, Cabuil V. Chem Mater 2001;13:3061.
[7] Schubert U. Chem Mater 2001;13:3487.
[8] Sanchez C. Prog Solid State Chem 2005;33:57.
[9] Mayer CR, Thouvenot R, Lalot T. Chem Mater 2000;12:257.
[10] Kickelbick G, Schubert U. Monatsh Chem 2001;132:13.
[11] Fric H, Schubert U. Z Naturforsch B J Chem Sci 2007;62:487–90.
[12] Moraru B, Kickelbick G, Schubert U. Eur J Inorg Chem 2001;5:1295–301.
[13] Moraru B, Gross S, Kickelbick G, Trimmel G, Schubert U. Monatsh Chem 2001; 132:993–9.
[14] Trimmel G, Gross S, Kickelbick G, Schubert U. Appl Organomet Chem 2001; 15:410.
[15] Gross S, Kickelbick G, Puchberger M, Schubert U. Monatsh Chem 2003; 134:1053–63.
[16] Schubert U. Acc Chem Res 2007;40:730–7.
[17] Fric H, Kogler FR, Puchberger M, Schubert U. Z Naturforsch B Chem Phys 2004; 59b:1241–5.
[18] Jupa M, Kickelbick G, Schubert U. Eur J Inorg Chem 2004;9:1835–9.
[19] Kogler FR, Jupa M, Puchberger M, Schubert U. J Mater Chem 2004;14: 3133–8.
[20] Palacio F, Oliete P, Schubert U, Mijatovic I, Hüsing N, Peterlik H. J Mater Chem 2004;14:1873–8.
[21] Schubert U. J Sol–Gel Sci Technol 2004;31:19–24.
[22] Schubert U, Bauer U, Fric H, Puchberger M, Rupp W, Torma V. Mat Res Soc Symp Proc 2005;847:533–9.
[23] Fric H, Jupa M, Schubert U. Monatsh Chem 2006;137:1–6.
[24] Puchberger M, Kogler FR, Jupa M, Gross S, Fric H, Kickelbick G, et al. Eur J Inorg Chem 2006;16:3283.
[25] Gao Y, Kogler FR, Peterlik H, Schubert U. J Mater Chem 2006;16:3268–76.
[26] Faccini F, Fric H, Schubert U, Wendel E, Tsetsgee O, Müller K, et al. J Mater Chem 2007;17:3297–307.
[27] Sanchez C, Schubert U, Laine R, Chujo Y. Inorganic–organic hybrid materials 2004. Warrendale, Pennsylvania: Materials Research Society, ISBN 1-55899-795-4; 2005.
[28] Schubert U, Völkel T, Moszner N. Chem Mater 2001;13:3811–2.
[29] Trimmel G, Moraru BA, Gross S, Di Noto V, Schubert U. Macromol Symp 2001;175:357–66.
[30] Gao Y, Choudhury N, Matisons J, Schubert U. Chem Mater 2002;14:4522–9.
[31] Sangermano M, Gross S, Priola A, Rizza G, Sada C. Macromol Chem Phys 2007; 208:2560–8.
[32] Gross S, Trimmel G, Schubert U, Di Noto V. Polym Adv Technol 2002;13: 254–9.
[33] Kickelbick G, Feth M, Bertagnolli H, Moraru BA, Trimmel G, Schubert U. Monatsh Chem 2002;133:919–29.
[34] Moraru B, Hüsing N, Kickelbick G, Schubert U, Fratzl P, Peterlik H. Chem Mater 2002;14:2732–40.
[35] Gross S, Di Noto V, Schubert U. J Non Cryst Solids 2003;322:154–9.
[36] Torma V, Hüsing N, Peterlik H, Schubert U. CR Chim 2004;7:495–502.

[37] Gao Y, Dragan SD, Jupa M, Kogler FR, Puchberger M, Schubert U. Mat Res Soc Symp Proc 2005;847:539–44.
[38] Gao Y, Kogler FR, Schubert U. J Polym Sci Part A Polym Chem 2005;43: 6586–91.
[39] Schubert U, Gao Y, Kogler FR. Prog Solid State Chem 2007;35:161–70; Koch T, Kogler FR, Schubert U, Seidler S. Monatsh Chem 2005;138:293–9; Kogler FR, Schubert U. Polymer 2007;48:4990.
[40] Schubert U. Polymers reinforced by covalently-bonded metal oxide clusters. In: Laine R, Blum F, editors. Organic/inorganic hybrid materials. American Chemical Society; 2003. p. 103–22.
[41] Sangermano M, Gross S, Pracella L, Priola A, Rizza G. Macromol Chem Phys 2007;208:1730–6.
[42] Di Maggio R, Campostrini R, Guella G. Chem Mater 1998;10:3839.
[43] Di Maggio R, Fambri L, Cesconi M, Vaona W. Macromolecules 2002;35:5342–4.
[44] Fauoassier JP, Rabek JC. Radiation curing in polymer science and technology, vol. I–IV. London: Elsevier; 1993.
[45] Roffey CG. Photopolymerisation of surface coatings. New York: Wiley; 1982.
[46] Gross S, Di Noto V, Kickelbick G, Schubert U. Mat Res Soc Symp Proc 2002; 726:Q4.1.1–4.1.9.
[47] Briggs D, Seah MP. Practical surface analysis. J. Wiley & Sons; 1990.
[48] Shirley A. Phys Rev B 1972;5:4709.
[49] Moulder JF, Stickle WF, Sobol PE, Bomben KD. In: Chastain J, editor. Handbook of X-ray photoelectron spectroscopy. Eden Prairie: Perkin Elemer Corp; 1992.
[50] NIST X-ray photoelectron spectroscopy database, version 3.5. Gaithersburg: National Institute of Standards and Technology; 2003. Available from: <http://srdata.nist.gov/xps/>.
[51] Armelao L, Gross S, Tondello E, Zattin A. Surf Sci Spectra 2005;10:157.
[52] (a) Armelao L, Eisenmenger-Sittner C, Groenewolt M, Gross S, Sada C, Schubert U, et al. J Mater Chem 2005;15:1838–48;
(b) Louette P, Bodino F, Pireaux JJ. Surf Sci Spectra 2005;12:64.
[53] Ertel TS, Bertagnolli H, Hückmann S, Kolb U, Peter D. Appl Spectrosc 1992; 46:690.
[54] Newville M, Livins P, Yacoby Y, Rehr JJ, Stern EA. Phys Rev B 1993;47:14126.
[55] Stern EA. Phys Rev B 1993;48:9825.
[56] Gurman SJ, Binsted N, Ross I. J Phys C 1984;17:143.
[57] Roy M, Gurman SJ. J Synchrotron Radiat 1999;6:228.
[58] Binsted N. Manual. In: Mosselman F, editor. EXCURV98: CCLRC Daresbury laboratory computer program; 1998.
[59] (a) Allen G, Bevington JC. Comprehensive polymer science – the synthesis, characterization, reaction and application of polymer. In: Booth C, Prince C, editors. Polymer properties, vol. 2. Pergamon Press; 1961;
(b) Helias HG. Makromoleküle. 5th ed. Basel: Hütig & Wepf Verlag; 1990.
[60] Moretti G, Guidi F, Canton R, Battagliarin M, Rossetto G. Anti-Corros Methods Mater 2005;52:266.
[61] Gross S, Zattin A, Di Noto V, Lavina S. Monatsh Chem 2006;137:583.
[62] Li P, Chen IW, Penner-Hahn JE. Phys Rev B 1993;48:10063–73.
[63] Sanchez C, In M. J Non-Cryst Solids 1992;147 and 148:1–12.
[64] Rose J, De Bruin TJM, Chauveteau G, Tabary R, Hazemann JL, Proux O, et al. J Phys Chem B 2003;107:2910–20.
[65] Winterer M, Delaplane R, McGreevy R. J Appl Crystallogr 2002;35:434–42.
[66] Mountjoy G, Pickup DM, Anderson R, Wallidge GW, Holland MA, Newport RJ, et al. Phys Chem Chem Phys 2000;2:2455–60.
[67] Mark HF, Bikales NM, Overberger CG, Menges G. Encyclopedia of polymer science and technology. New York: John Wiley and Sons; 1985.
[68] Kogler FR, Koch T, Peterlik H, Seidler S, Schubert U. J Polym Sci Part B Polym Phys 2007;45:2215–31.
[69] Diez-Gutierrez S, Rodriguez-Perez MA, De Saja JA, Velasco JJ. Polymer 1999; 40:5345.
[70] Girardi F, Graziola F, Aldighieri P, Fedrizzi L, Gross S, Di Maggio R. Prog Org Coat 2008;62:376–81.